HiSST: 2nd International Conference on
High-Speed Vehicle Science & Technology
11–15 September 2022, Bruges, Belgium

Numerical Investigation of Ground Heat Fluxes from Supersonic Jet Impingement during Vertical Landing of a Reusable First Stage Demonstrator

Moritz Ertl[1], Yannik Feldner[1], Tobias Ecker[1]

Abstract

Several actors in the space trasport sector are moving towards reusable launch vehicles (RLV) for the first stages of launchers, among them SpaceX with the Falcon 9 [1] and Rocket Lab with the Neutron [2]. Also the current European long term strategy [3] is aiming towards reusability with plans for THEMIS [4] and Ariane Next [5]. In accordance with this strategy the German Aerospace Center (DLR) has entered into a collaboration with the Japan Aerospace Exploration Agency (JAXA) and the French Space Agency (CNES) for the development of RLV relevant technologies in the frame of a vertical take-off and vertical landing (VTVL) reusable subscale launcher first stage demonstrator - the "Cooperative Action Leading to Launcher Innovation in Stage Toss back Operations" (CALLISTO) [6, 7].
Generally a VTVL first stage will return to the launch pad utilising retro-propulsion and an Approach and Landing System (ALS) [8] with deployable landing legs. The landing leads to new additional aerothermal design questions compared to traditional launchers. It has been observed, that part of the critical heat loads are happening after touch down and engine shut off. These are caused by heat radiation from the launch pad to the vehicle structure. This can affect an ALS built from carbon fibre, which is prevented from cooling down. The heat fluxes, therefore, influence the structural design and the thermal protection system (TPS) of the ALS. The impact is even more relevant to experimental vehicles if hopper flights are part of the program.
To aid the development of reusable launch vehicles in the VTVL configuration we analyse the heat fluxes onto the ground for an impinging supersonic jet from a liquid hydrogen and oxygen engine. The analysis is based on Reynolds averaged Navier-Stokes computational fluid dynamics. We look at some modelling choices and we investigate the influence of the ground distance on the heat flux distribution.

Keywords: *reusable launch vehicle, VTVL, retro-propulsion, aerothermal, CFD, RANS, ground heat flux, jet impingement, supersonic jet*

Nomenclature

Latin

D_{NE} – nozzle exit diameter [m]
x/D – distance nozzle to ground [m]
z/D – radial coordinate [m]
T – temperature [K]
T_w – wall temperature [K]
h – area specific heat flux [W m^{-2}]
Ma – Mach number [$-$]
ofr – oxidise to fuel ratio [$-$]
p – pressure [Pa]

1. Introduction

Space launches are know to be expensive. One of the reasons for this is that conventional launch vehicles are only single use. A way of reducing the cost of launches might be to reuse costly parts of the vehicle, which has been of interest since the last century [9] and has been demonstrated by SpaceX with the first stage of the Falcon 9 rocket [1]. Europe and Japan, while they are finalising the development efforts for their new conventional launcher generations, have started the research and development on reusable launch vehicles in a cooperation. The "Cooperative Action Leading to Launcher Innovation in

[1]*German Aerospace Center (DLR), Institute of Aerodynamics and Flow Technology, Department Spacecraft, moritz.ertl@dlr.de, tobias.ecker@dlr.de*

Stage Toss back Operations" (Callisto) [6] vehicle is a flight demonstrator by CNES, DLR and JAXA, for future reusable launcher stages and the relevant technologies. Callisto is a first stage demonstrator for a vertical take-off and vertical landing (VTVL) space transport system with a single liquid hydrogen-oxygen engine. Its mission is to vertically launch and return the single stage vehicle to the launch pad. For the return flight the demonstrator employs a phase of glide, during which the drag is used to break the vehicle, followed by the re-ignition of the liquid hydrogen and oxygen engine and and retro-propulsion breaking before utilising its Approach and Landing System (ALS) [8, 10] with deployable legs to land on the landing pad. At heights close to the ground the nozzle of the Callisto vehicle is over-expanded. Prior to the mission some shorter test flights and hops are planned for validation and proof of flight worthiness. While the presented work was produced in the context of Callisto the results are applicable to general reusable VTVL launcher such as the Rocket Lab Neutron [2] or the ArianeGroup projects THEMIS [4] and Ariane Next [5].

One important aspect in vertically landing RLVs are the heat fluxes onto the ground. During the vehicles approach to the ground for landing or in case of hopper tests, the hot exhaust jet from the retro-propulsion can lead to significant heat transfer to the vehicle structure, especially the landing legs. One cause of this heat transfer can be the direct plume-vehicle-interaction, which the authors have investigated in previous publications [7, 11–13]. An additional cause can be the heating of the ground/landing pad by the hot engine plume, which then in return heats up the vehicle due to radiation. This can lead to damaging temperature levels inside the vehicle structures. When designing a VTVL RLV it is, therefore, important to correctly estimate these heat fluxes. The impact is even more relevant to experimental vehicles if hopper flights are part of the program. The investigated mechanisms can also be considered a special case of jet impingement on an inclined plate as is often found in a flame trench.

Experimental investigations of the ground heat fluxes are difficult to conduct, due to the extreme conditions of the jet. Furthermore, experimental investigations of a large parameter space are prohibitive due to cost. Therefore, numerical simulations are chosen for this investigation. While subsonic impingement jets are already well researched [14, 15], the research on supersonic impingement jets is still rather sparse. The impingement of a supersonic jet onto a flat plate has been experimentally investigated by Gummer and Hunt [16]. They used shadowgraphy to observe the jet structure and measured the pressure onto the plate. They compared these results to analytical predictions. For ground distances smaller than the free stream extension a deflection of the shock structures onto the wall was observed, exhibiting subsonic, transsonic and supersonic flow regions. Klinkov [17] investigated supersonic jets impingement both experimentally and theoretically. The jets are particle laden and impinge normally onto a flat plate. The jet has a Mach number $Ma = 2.6 - 2.8$ and stagnation temperatures of $T = 300 - 500$K. The analysis focused on flow oscillations as well as on particle-surface interactions and the physical mechanisms, including the recirculation and the shock structures are explained. Alvi et al. [18] experimentally and numerically investigated under-expanded supersonic jets for STOVL aircrafts. They used PIV and CFD to investigate the relevant flow features focusing on the recirculation in the stagnation bubble. They measured and analysed the pressure distribution on the plate. They compared the performance of different turbulence models and obtained a good agreement with experimental data for the SST and the SARC turbulence model while the SA model proved less suited for the problem.

Investigations of the thermal loads from the impinging supersonic jets were done by the group of Kim et al. [19, 20] and Yu et al. [21]. They experimentally investigated under-expanded jets impinging onto a normal plate and measured plate pressure and heat fluxes for different pressure ratios and different distances. The heat fluxes are provided as non-dimensional Nusselt number or recovery factor. They additionally used shadowgraphy to visualise the jets. While they provided a good quantitative overview for different parameters, their results sadly could not be used for a validation, as they did not provide the heat flux applied to their heated foil for the heat flux measurements. Tian et al. [22] numerically investigated under-expanded supersonic impinging jets. They investigated different plate distances and pressure ratios and looked into turbulence models and multi species modelling. They used validation versus experimental data from an blunt conical head to investigate the turbulence models and decided on the use of the SA model. This paper provides an overview of some numerical options and parameters for under-expanded supersonic impingement jets, but since the Callisto nozzle is over-expanded for heights

close to the ground an additional investigation for this setup was necessary.

The aim of this work is to investigate the ground heat fluxes for different heights over ground for an over-expanded H_2/O_2 engine. We aim to investigate the flow field and its influence on heat transfer. Additionally the influence of different modelling rigour, especially the influence of chemical modelling, on the accuracy of the heat flux prediction is analysed.

2. Numerical Method

The numerical simulations for this work are done using the DLR TAU code [23]. The TAU code is a finite volume CFD code solving the Reynolds Averaged Navier Stokes (RANS) equations. It can solve 2D and 3D problems on hybrid structured-unstructured dual grid meshes. The simulations are 2nd order accurate in time and space using the upwinding difference scheme AUSMDV [24] and a least squares reconstruction for the gradients. The temporal discretisation is done with a backward Euler scheme. For regions of low Mach numbers a modification for the variable reconstruction proposed by Thornber [25] is used to improve numerical accuracy. The equation system is solved using a multigrid solver. A selection of turbulence models is available, of which the two equation $k-\omega$ model by Wilcox et al. [26] is used for the simulations. All presented simulations are stationary converged RANS.

The modelling of the rate change of species due to post combustion can be modelled using a finite rate chemistry approach. The rate at which each species changes during a chemical process is determined from the chemical reactions as formulated in Hannemann [27]:

$$\omega_s = M_s \sum_r \left(\beta_s^r - \alpha_s^r\right) \left[k_r^f \prod_s \left(n_s\right)^{\alpha_s^r} - k_r^b \prod_s \left(n_s\right)^{\beta_s^r}\right]$$

where α_s^r and β_s^r are the stoichiometric coefficients for the educt and product for reaction r respectively, k_r^f and k_r^b the forward and backward reaction rate for reaction r respectively, n_s is the molar density and M_s is the molar mass of species s. k_r^f is the forward reaction rate according to the Arrhenius law

$$k = A\ T^n \exp\left(-\frac{E_a}{RT}\right)$$

where A is the pre-exponential factor, n is the temperature exponent and E_a is the activation energy. The rate constants k_b^f for the reverse reactions are evaluated from the equilibrium constants. The model used here is the reduced Jachimowsky mechanism [28]. A more detailed overview of the reactions and the modelling can be obtained from Ecker et al. [12]. The suitability of TAU code for the numerical prediction of heat fluxes in high speed flows is documented in [29].

The simulations are set up with a 2D axisymmetrical mesh which is shown in figure 1. The axisymmetric wedge has an angle of $1°$ and a large far field of $2800D$ was chosen to prevent problems with back flow. The nozzle with diameter $D = 268.318$mm as well as the grid refinement in the near nozzle area are shown in figure 1b. The jet flow is exiting the nozzle boundary condition - a Dirichlet BC - along the symmetry axis in negative x direction and is impinging normally onto the ground, which is oriented in z direction and modelled as a viscous wall with a wall temperature of $T_w = 300$K.

The computational domain is initialised with air with a density of $\rho_{ref} = 1.2$kg m^{-2} and a temperature of $T_{ref} = 300$K. The reference conditions are also applied to the far field boundary condition and a very low velocity of $Ma = 1 \times 10^{-2}$ is set in negative x direction for reasons of computational stability.

The cell size for the first layer is chosen such, that a dimensionless wall distance of $y^+ < 1.0$ is achieved. The grid used for the computations is called the medium grid and has over 800.000 cells. A grid convergence index (CGI) study using the methodology proposed by Celik et al. [30] was done. A coarser and a finer mesh were generated scaled with refinement factors of about $r \approx 1.3$ compared to the medium grid. The results are shown in figure 2. The visualisation for the ground heat flux in 2a for the three grids shows a good agreement for the chosen meshes, as all three are already rather fine due to the

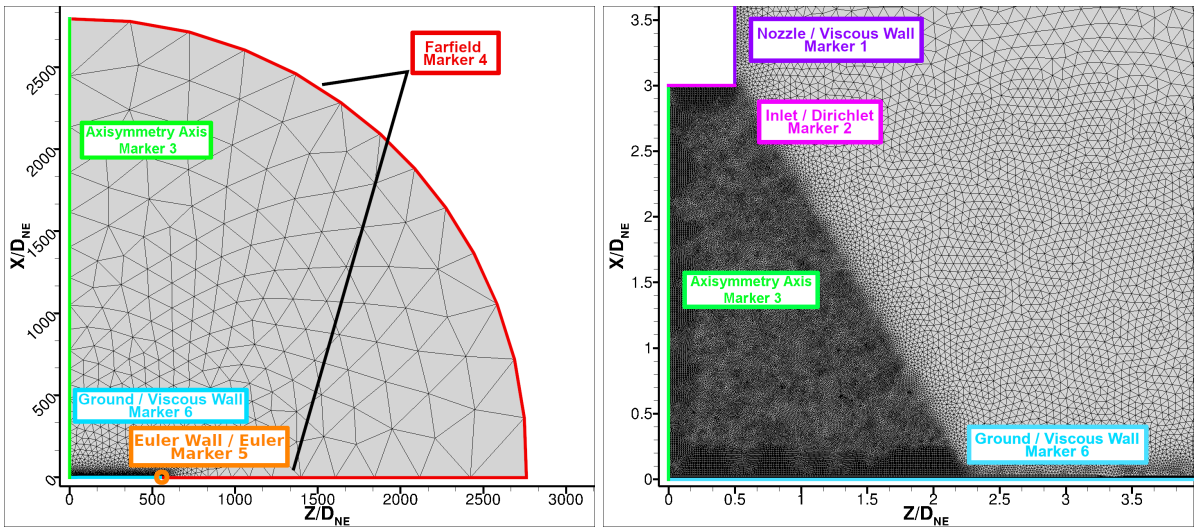

(a) Complete view of the Mesh with a large far field. **(b)** Mesh section with nozzle and grid refinement

Fig 1. Visualisation of the 2D axisymmetric computational mesh (medium) including labelling of the relevant boundary conditions.

constrains from the dimensionless wall distance. The compared grids are generally within the error bars, especially in the radial close range of $0 - 10D$. The results of the GCI are provided in the table 2b. The ϵ values are rather close to each other. Both the e values and the heat flux curves indicate oscillatory convergence. This can be seen from the heat fluxe curves for the different grids, which are intersecting in the relevant region due to their similarity. Therefore, the percentage occurrence for oscillatory convergence is calculated. With an oscillatory occurrence of over 80% for the close range indicates, it is assumed that despite the calculated $CGI^{21}_{fine} = 0.28$ the chosen mesh is sized well.

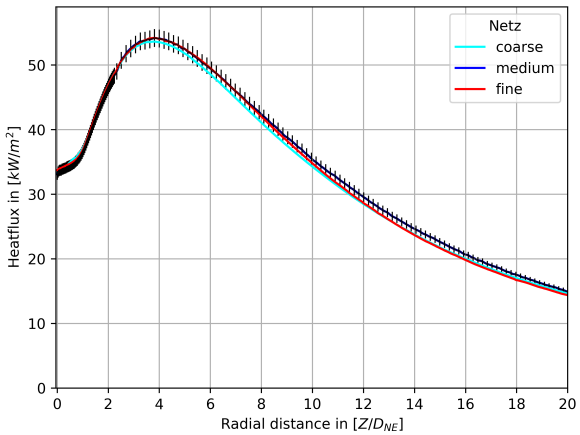

(a) Comparison of heat fluxes on the ground for three different mesh sizes, including error bars.

mean error in %	close range ground	groundplate
e^{21}_a	2.16	2.56
e^{21}_{ext}	0.23	1.19
$\text{GCI}^{21}_{\text{fine}}$	0.28	1.46
e^{32}_a	1.00	2.89
e^{32}_{ext}	0.18	1.57
$\text{GCI}^{32}_{\text{coarse}}$	0.22	1.91
oscillatory conv. in %	89.7	46.04
apparent order p	9.46	25.93

(b) Table with the CGI results

Fig 2. Results of the grid convergence index for the computational mesh.

3. Results

3.1. General Flow Field Observations

The 2D axisymmetric case of $x/D = 3.0$, with two species and frozen chemistry, the Wilcox $k-\omega$ turbulence model and a real nozzle velocity profile is chose as reference case and is used to give a general description of the flow field. A more detailed description of the real nozzle velocity profile is provided in section 3.2.1 and of the two species and frozen chemistry in section 3.2.2. The flow field is visualised in figure 3 with a) Mach field and stream lines and b) temperature field.

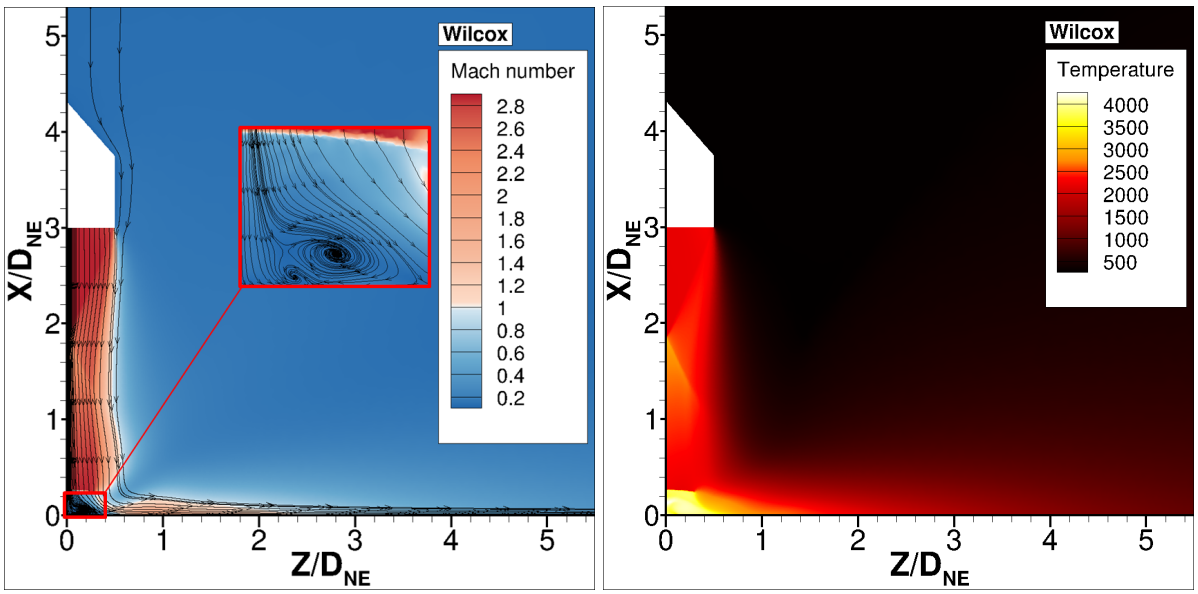

(a) Mach field with stream lines and a magnified view of the recirculation in the stagnation region.

(b) Temperature field

Fig 3. Flow field visualisation for reference case: 2D axisymmetric impingement jet with ground distance $x/D = 3.0$, two species frozen chemistry, real nozzle velocity boundary condition and Wilcox $k-\omega$ turbulence model.

First we analyse the vertical part of the jet in the radial region of $z/D = 0 - 0.5$. The Mach field shows the jet entering the domain from the nozzle BC with $Ma \approx 3$. The jet exhibits a classical diamond shaped shock structure [31] in the region $x/D = 3.0 - 1.0$. Just before impinging onto the ground at hight $x/D \approx 0.3$ the jet forms a horizontal bow shock, the plate shock, with a stagnation region with recirculation. At the far radial end of the plate shock the supersonic slip line moves across towards the ground. The jet velocity reaches zero with a corresponding increase in pressure. Due to this higher pressure after impinging onto the the ground the jet is deflected in radial direction and accelerated along the ground forming a wall jet. The wall jet is the horizontal part of the jet and is found in the region $x/D < 0.5$ for $z/D > 0.5$. In the presented case the pressure in the stagnation region is high enough to accelerate the wall jet to supersonic speeds, exhibiting a second region with $Ma > 1$ directly to the right of the stagnation region. For radial distances over $z/D > 2.4$ the velocities become subsonic. The recirculation region below the plate shock is shown magnified in the inlay in figure 3a.

The temperature field shown in figure 3b exhibits the same shock patterns in the jet as seen in the Mach plot. The jet enters the domain with a temperature of about $T \approx 2300$K. The maximum temperature is observed in the stagnation region with temperatures close to $T \approx 4000$K. In the wall jet the temperature decreases with radial distance z/D.

3.2. Investigation of Modelling Fidelity

We investigated the effects of different choices in modelling fidelity on the simulation results. The modelling choices and the resulting flow fields as well as the heat fluxes are presented for two influences:

fidelity of the inflow boundary condition and chemical reactions for post combustion. All investigations are done with the reference case with a nozzle to ground distance of $x/D = 3$ and the Wilcox $k-\omega$ turbulence model. A matrix with the short names for the four investigated cases is provided in table 1. The modelling choices are explained in more detail in the following two sections.

Table 1. Investigated modelling options and short names

	nozzle with constant inflow variables distribution of averaged properties	real velocity nozzle profile with interpolated distribution of properties
2 mixture species with frozen chemistry	2 species, homogeneous nozzle	2 species, interpolated nozzle
10 molecule species with post combustion modelling	10 species, homogeneous nozzle	10 species, interpolated nozzle

3.2.1. Influence of Inflow Boundary Condition

Two different ways of defining the inflow boundary condition are investigated. The nozzle inflow is set up as a Dirichlet boundary condition. For both cases the combustion chamber conditions are calculated in chemical equilibrium with NASA CEA [32]. The combustion chamber conditions for the simulations are a mixture of liquid hydrogen and oxygen with an oxidiser to fuel ratio $ofr = 6$, a chamber pressure of $p_{cc} = 34$bar and a chamber temperature of about $T_{cc} \approx 3500$K. With these conditions a stationary 2D axisymmetric nozzle simulation including chemical combustion modelling is run.

In the simpler case - called the homogeneous nozzle - a constant distribution of inflow variablesis used obtained from the averaged results of the nozzle simulation for pressure and temperature etc. as well as the post combustion species composition at the nozzle exit. In the higher fidelity case - the interpolated nozzle case - all relevant parameters at the nozzle exit (i.E. velocity, species composition pressure, temperature) are interpolated onto the Dirichlet boundary condition of the jet impingement simulation.The mass fractions Y_i for the most prevalent species at the outflow of the nozzle simulation are given in table 2.

Table 2. Mass fractions of the most prevalent combustion products for the nozzle simulation outflow.

species i	H_2	O_2	H_2O	OH	H	O
Y_i	1.86×10^{-2}	9.43×10^{-4}	9.72×10^{-1}	7.83×10^{-3}	4.08×10^{-4}	1.95×10^{-4}

A comparison between the flow fields of the two inflow boundary conditions is shown in figure 4 with the constant variable distribution on the left side. The influence of the nozzle velocity profile can be observed in a less steep angle of the nozzle shock due to the lower velocity gradients in the shear layer. Further differences can be seen in the stagnation region. The bow shock exhibits a bigger distance to the ground, there are differences in the flow of the recirculation and the slip lines are differently shaped. The corresponding heat fluxes are described in section 3.2.3

3.2.2. Influence of Species and Chemistry Modelling

The influence of post combustion modelling on the simulation fidelity has been investigated. The case named 2 species uses two gas mixtures modelled as single species with the physical properties of the mixture. The first species is dry air. The second is representing the exhaust gases obtained by combining the species from the nozzle simulation averaged at the nozzle exit into one mixture. The nozzle simulation is described in more detail in section 3.2.1. In the case named 10 species, all the species from the nozzle simulation are interpolated onto the Dirichle boundary condition and transported through the computational domain. Reactions between these species and with the components of air are modelled according to the description in section 2.

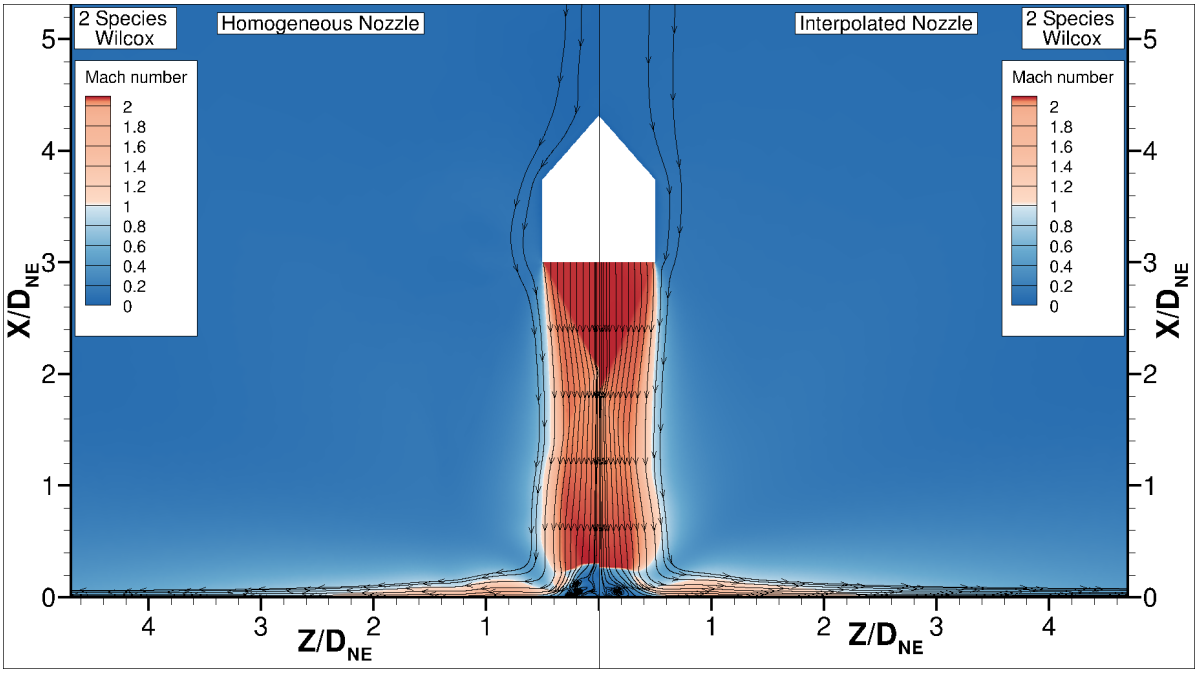

Fig 4. Comparison of the flow fields for different fidelity nozzle inflow boundary condition modelling. Ground distance $x/D = 3.0$ reference case, two species frozen chemistry and Wilcox $k-\omega$ turbulence model. On the left a nozzle with constant inflow variables distribution and on the right with a distribution interpolated from additional nozzle simulation.

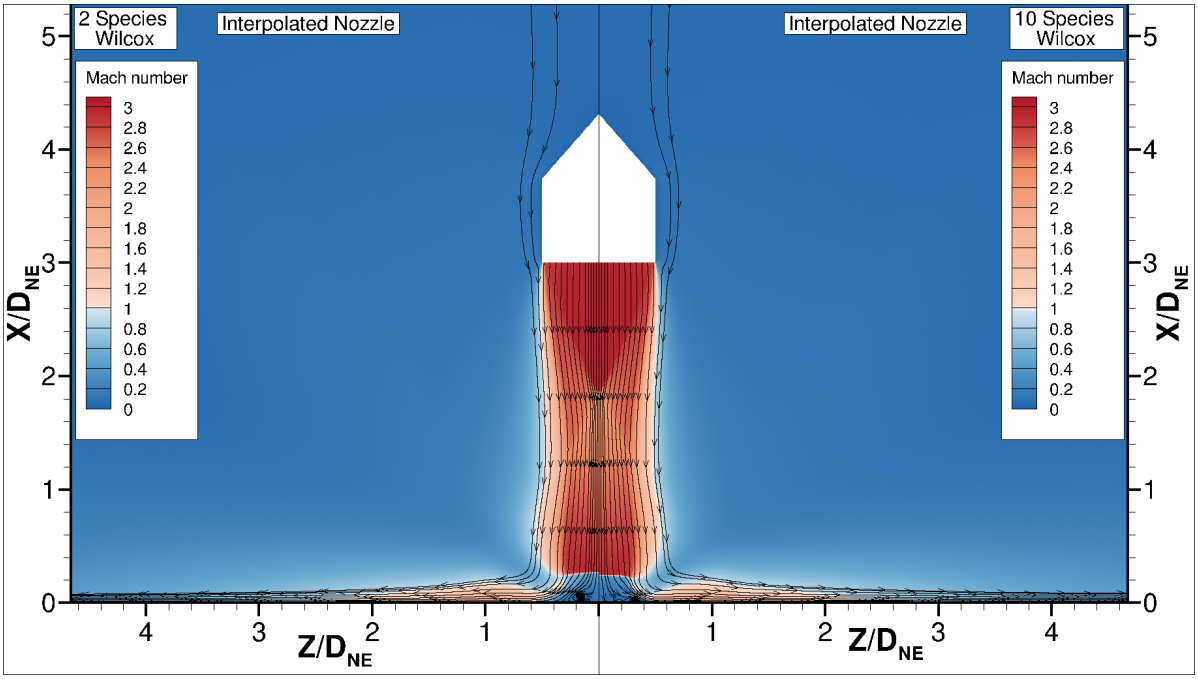

Fig 5. Comparison of the flow fields for different fidelity chemistry modelling. Ground distance $x/D = 3.0$ reference case, interpolated nozzle case and Wilcox $k-\omega$ turbulence model. On the left two species (air + exhaust) simulation with frozen chemistry and on the right 10 species with combustion modelling.

A comparison for the flow field of the case with frozen chemistry and the case with post combustion is shown in figure 5. The visible differences between the two cases are minor. The bow shock distance to the ground is slightly decreased for the post combustion, as is the centre point of the recirculation. This is not very surprising, as the mass fraction of H_2 is already below $Y_{H_2O} < 2 \times 10^{-2}$ at the nozzle exit, thus not providing much fuel for post combustion.

3.2.3. Heat Flux Comparison for the Modelling Investigation

The radial heat flux distribution on the ground for the two modelling investigations is given in figure 6. The post combustion simulations exhibit their maxium at $z/D \approx 0.5$ and have higher and less smooth heat fluxes in the stagnation region. We are stil investigating whether this is due to position of the recirculation region or whether it could be caused by recombination of some of the reacting species at the low wall temperature ground as described in [33]. The cases with post combustion also have the highest and the lowest heat fluxes despite having very similar flow fields as discussed in 3.2.2. The heat fluxes for the frozen chemistry cases are in between and have their maxima further towards the stagnation point as well as generally lower and smoother heat fluxes in the stagnation region.

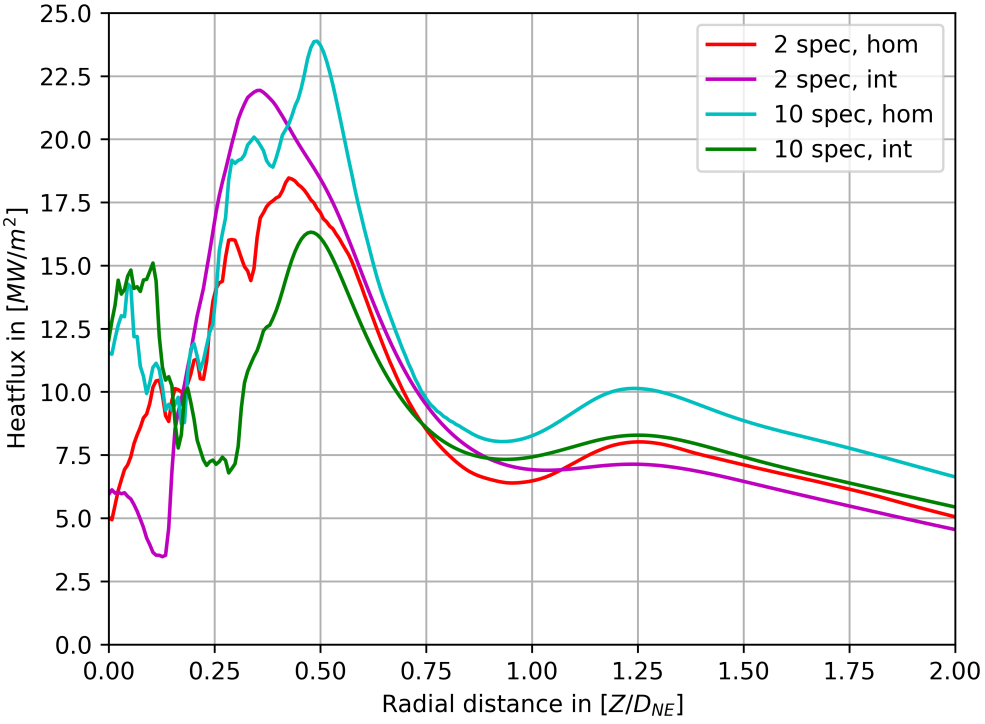

Fig 6. Comparison of the radial heat flux distribution for different modelling fidelity. Ground distance $x/D = 3.0$ reference case and Wilcox $k - \omega$ turbulence model.

The use of a nozzle with constant inflow variables distribution compared to a real variable distribution does not provide a clear trend for the heat fluxes. In the frozen chemistry case the heat flux maximum for the real nozzle profile exceeds the one for the constant inflow variable distribution, while in the case of post combustion it is the other way around. Without a comparison to experiments, for which we were not able to find usable data, a definitive choice in modelling depth is difficult. For our simulations we chose to use the combination of frozen chemistry and the real nozzle velocity profile boundary condition. This setup seems provide a conservative estimate of the heat fluxes, while being less computationally costly and providing better convergence behaviour.

3.3. Nozzle to Ground Distance

The flow field with Mach number and stream lines for the impingement jets for different nozzle to ground distances is shown in figure 7 for six nozzle to ground distances x/D. The simulations are done with

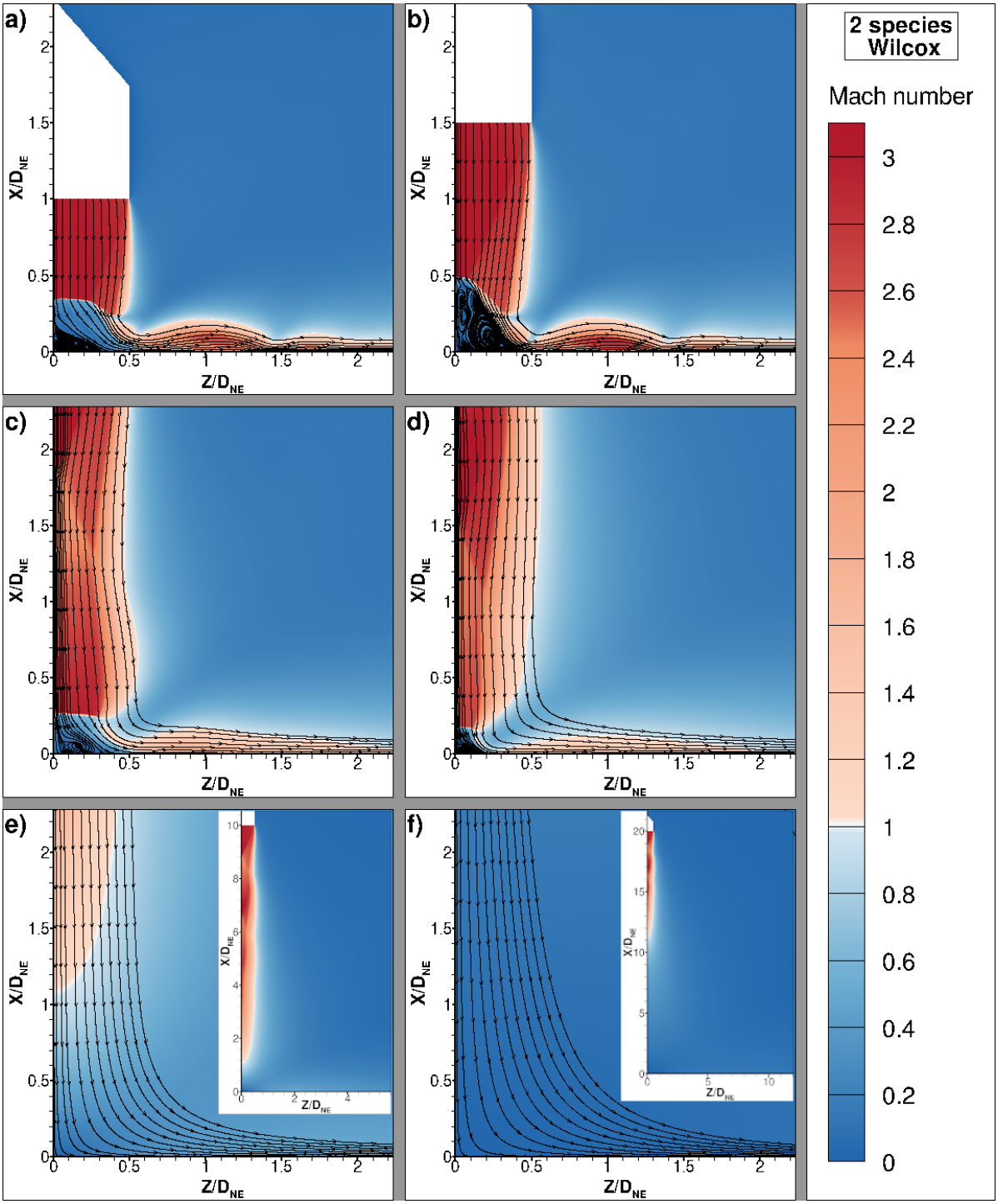

Fig 7. Mach field with stream lines for different heights: a) $x/D = 1$, b) $x/D = 1.5$, c) $x/D = 3$, d) $x/D = 5$, e) $x/D = 10$ and f) $x/D = 20$.

the nozzle velocity profile inflow boundary conditions and with two species and frozen chemistry. The distances $x/D = 20$ and $x/D = 10$ are shown in the last two visualisations e) and f). Here the distance to the ground exceeds the length of the supersonic jet. In both cases the a classical supersonic jet with shock cells can be seen. The jet reaches subsonic speeds prior to impingement onto the ground and thus at ground level exhibits the behaviour of a classical subsonic impingement jet.

For smaller nozzle to ground distances a recirculation in the stagnation region and a supersonic wall jet can be observed, as already described in more detail in section 3.1. The corresponding wall pressure distributions are shown in figure 8. The cases $x/D = 20$ and $x/D = 10$ are in the lower plot and exhibit a simple subsonic impingement jet pressure distribution with a maximum in pressure in the stagnation point $z/D = 0$ and a monotonic decrease in radial direction. Additionally the pressures are over a factor four lower compared to the other cases.

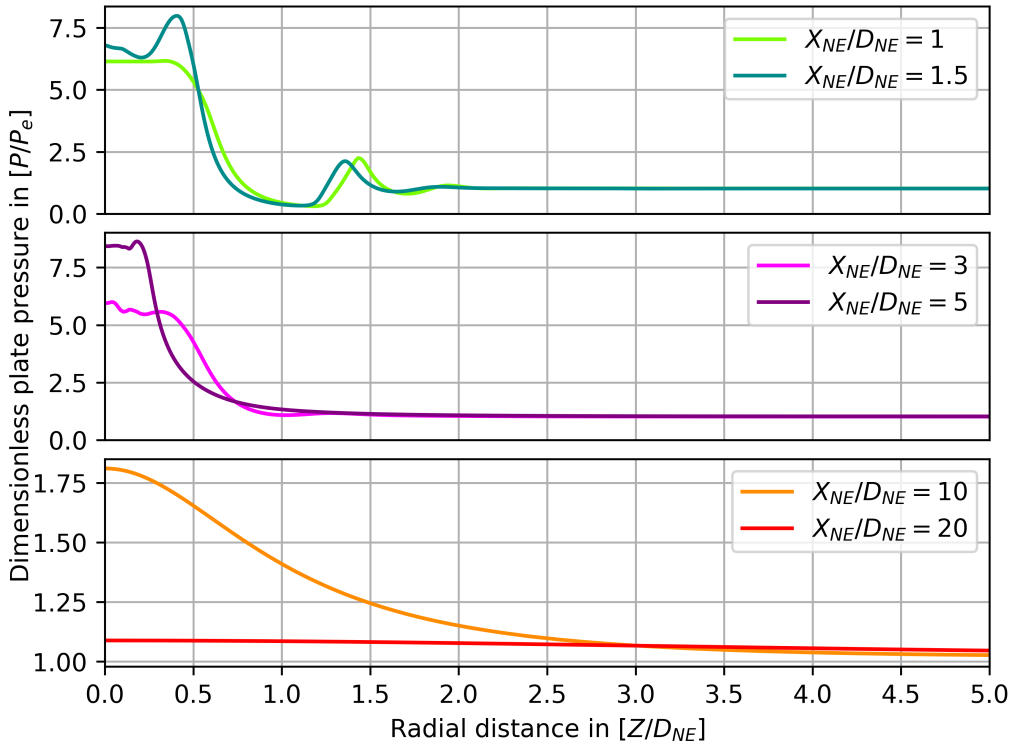

Fig 8. Dimensionless plate pressure distribution for different nozzle to ground distances.

The smaller nozzle to wall distances are shown in the middle for distances d)$x/D = 5$ and c)$x/D = 3$ and on the top for distances a)$x/D = 1.5$ and b)$x/D = 1.0$. The pressure maxima for these cases are more complex either with a pressure plateau or with the maximum shifted in radial direction towards the maximum extension of the subsonic region. These maxima are due to the flow structure, occurring at the point where the slip flow from the plate shock impinges onto the ground. These pressure distributions are theorized to be the cause of the recirculation in the stagnation region. The higher pressure outside the stagnation point causes a backflow towards the stagnation region, thus starting the recirculation. In the case of a)$x/D = 1.5$ and b)$x/D = 1.0$ a secondary peak in pressure can be observed at $z/D \approx 1.4$. This peak corresponds to an oblique shock in the wall stream which is also well visible in the flow fields in figure 7 and is due to the higher velocities in the wall jet for the closer distances.

The radial distribution of the heat flux to the ground is shown in figure 9 for the investigated nozzle to ground distances. The heat flux for the distances $x/D = 20$ and $x/D = 10$, shown in the lower plot, behaves analogous to the pressure distribution and in accordance with a classical subsonic impingement jet. The maximum is occurring in the stagnation point and reaches $h = 4.3\text{MW m}^{-2}$ for $x/D = 10$.

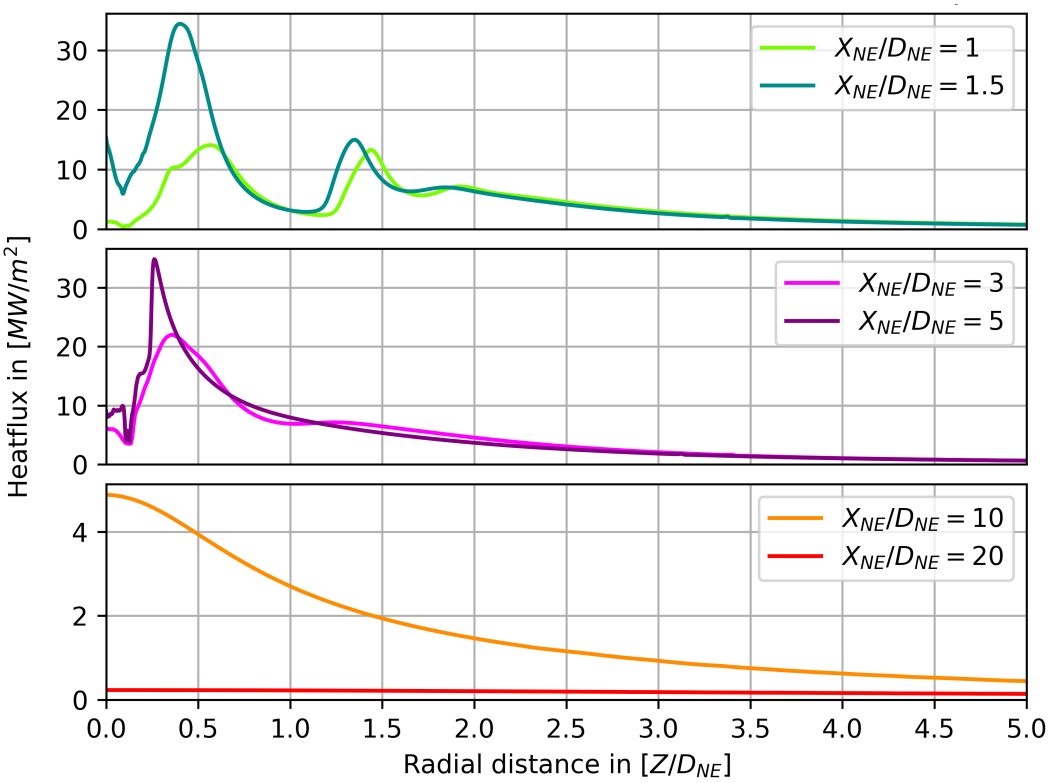

Fig 9. Heat flux distribution for different nozzle to ground distances.

For the jets with the lower distance the heat flux maxima are also outside of the stagnation point and are closely positioned to the pressure maxima. In contrast to a subsonic impingement jet the heat flux does not allow for the definition of an easy scaling law over distance. The cases $x/D = 5$ and $x/D = 1.5$ are exhibiting the highest maxima of over $h > 32\text{MW}\,\text{m}^{-2}$. $x/D = 3$ has a maximum of $h \approx 22\text{MW}\,\text{m}^{-2}$ and $x/D = 1$ has a maximum of $h \approx 15\text{MW}\,\text{m}^{-2}$, both clearly exceeding the subsonic impingement but below the highest maxima. Additionally the closes cases, $x/D = 1.5$ and $x/D = 1.0$ have a second peak in the heat flux of $h \approx 15\text{MW}\,\text{m}^{-2}$ at radial distance $z/D \approx 1.4$, coinciding with the shock in the wall jet and the secondary pressure peak.

4. Conclusions

We did computational fluid dynamics stationary Reynolds averaged Navier Stokes simulation of supersonic impingement jets from an overexpanded nozzle. The simulations were done in the context of Callisto to predict the heat fluxes to the landing pad for a vertically landing reusable first stage, but results should generally be applicable to any reusable VTVL first stage. We described the numerical method as well as the numerical setup and investigated the influence of different modelling fidelity on the flow field and predicted heat flux. The results, while not indicating a clear trend, showed lowest predicted heat fluxes for the highest fidelity. We chose a setup with a 2 species frozen chemistry for being computationally efficient, providing good convergence and for providing a conservative prediction.

We analysed the heat fluxes to the ground for different nozzle to ground distances x/D, investigating the flow field, the plate pressure and the radial heat flux distribution on the ground. We observed different regimes: For z/D greater than the length of the supersonic jet core the jet impinging onto the ground is subsonic and has the behaviour of a classical impingement jet. If x/D becomes smaller the supersonic part of the flow interacts with the ground and influences the stagnation region and the wall jet. This causes a large increase of the heat transfer with heat flux maxima increasing from

$h_{x/D=10} \approx 4.3$MW m^{-2} to $h_{x/D=5} \approx h_{x/D=1.5} \approx 32$MW m^{-2}. In this regime the flow structure and heat flux distributions become a lot more complex. The maxima in heat flux and pressure are shifted in radial direction. We observed recirculation flows in the stagnation region, which is assumed to be caused by the shifted pressure maxima as described in Klinkov [17]. If x/D is reduced even further additional smaller heat flux maxima occur in radial direction z/D.

The complex flow structure, as indicated by the different regimes, makes interpolation for heat flux prediction or aerothermal engineering databse creation problematic. Our recommendation is to try to best avoid these cases, which only occur close to the ground, by either shutting off the engine prior to reaching these distance, or by landing on a grid, or by keeping the time of this part of the operation short.

References

1. Blackmore, L. *Frontiers of Engineering: Reports on Leading-Edge Engineering from the 2016 Symposium* in, 33–41 (The National Academies Press, Washington, DC, 2017).
2. Callsen, S. *Critical Analysis of Rocket Lab Neutron Launcher and Missions* tech. rep. (Mar. 2022).
3. Préaud, J.-P., Dussy, S., Breteau, J. B. & Bru, J. B. *Preparing the Future of European Space Transportation: Reusable Technologies and Demonstrators* in *8th European Conference for Aeronautics and Space Sciences (EUCASS), Madrid, Spain* (July 2019).
4. Simontacchi, P., Blasi, R., Edeline, E., Sagnier, S., Ravier, N., Espinosa-Ramos, A., Breteau, J. & Altenhoefer, P. *PROMETHEUS: Precursor of new low-cost rocket enginefamily* in *8TH EUROPEAN CONFERENCE FOR AERONAUTICS AND SPACE SCIENCES (EUCASS)* (2019).
5. De Mirand, A. P., Bahu, J.-M. & Louaas, E. *Ariane Next, a vision for a reusable cost efficientEuropean rocket* in *8TH EUROPEAN CONFERENCE FOR AERONAUTICS AND SPACE SCIENCES (EUCASS)* (2019).
6. Dumont, E., Ishimoto, S., Tatiossian, P., Klevanski, J., Reimann, B., Ecker, T., Witte, L., Riehmer, J., Sagliano, M., Vincenzino, S. G., Petkov, I., Rotärmel, W., Schwarz, R., Seelbinder, D., Markgraf, M., Sommer, J., Pfau, D. & Martens, H. *CALLISTO: a Demonstrator for Reusable Launcher Key Technologies* in *32nd International Symposium on Space Technology and Science (ISTS)* (Fukui, Japan, June 2019).
7. Krummen, S., Desmariaux, J., Saito, Y., Boldt, M., Briese, L. E., Cesco, N., Chavagnac, C., Cliquet-Moreno, E., Dumont, E., Ecker, T., Eichel, S., Ertl, M., Giagkozoglou, S., Glaser, T., Grimm, C., Illig, M., Ishimoto, S., Klevanski, J., Lidon, N., Mierheim, O., Niccolai, J.-F., Reershemius, S., Reimann, B., Riehmer, J., Sagliano, M., Scheufler, H., Schneider, A., Schröder, S., Schwarz, R., Seelbinder, D., Stief, M., Windelberg, J. & Woicke, S. *Towards a Reusable First Stage Demonstrator: CALLISTO - Technical Progresses & Challenges* in *72th International Astronautical Congress (IAC)* IAC-21-D2.6.1 (Oct. 2021).
8. Vincenzino, S. G., Rotärmel, W., Petkov, I., Elsäßer, H., Dumont, E., Witte, L. & Schröder, S. *Reusable Structures for CALLISTO* in *8th European Conference for Aeronautics and Space Sciences (EUCASS)* (July 2019).
9. Koelle, D. & Kuczera, H. Sänger II, an advanced launcher system for Europe. *Acta Astronautica* **19,** 63–72 (1989).
10. Vincenzino, S. G., Eichel, S., Rotärmel, W., Krziwanie, F., Petkov, I., Dumont, E., Schneider, A., Schröder, S., Windelberg, J., Ecker, T. & Ertl, M. *Development of Reusable Structures and Mechanisms for CALLISTO* in *33rd ISTS Conference* (Mar. 2022).
11. Ertl, M., Ecker, T., Klevanski, J., Krummen, S. & Dumont, E. *Aerothermal analysis of plume interaction with deployed landing legs of the CALLISTO vehicle* in *9th European Conference for Aeronautics and Space Sciences* (2022).
12. Ecker, T., Ertl, M., Klevanski, J., Dumont, E. & Krummen, S. *Aerothermal characterization of the CALLISTO vehicle during descent* in *9th European Conference for Aeronautics and Space Sciences* (2022).
13. Ecker, T., Karl, S., Dumont, E., Stappert, S. & Krause, D. Numerical Study on the Thermal Loads During a Supersonic Rocket Retropropulsion Maneuver. *Journal of Spacecraft and Rockets* **57,** 1–16 (Jan. 2020).

14. Brakmann, R. G. *Increasing Heat Transfer in Convective Cooling Systems withOptimized Surface Structures* PhD thesis (University of Stuttgart, 2017).
15. Hofmann, H. M. *Wärmeübergang beim pulsierenden Prallstrahl* PhD thesis (Karlsruhe Institute of Technology, 2005).
16. Gummer, J. H. & Hunt, B. L. The Impingement of a Uniform, Axisymmetric, Supersonic Jet on a Perpendicular Flat Plate. *Aeronautical Quarterly* **22,** 403–420 (1971).
17. Klinkov, K. V. *Unsteady gas flows and particle dynamics in the shock layer formed by the impingement of a supersonic two-phase jet onto a plate* PhD thesis (University of Göttingen, 2005).
18. Alvi, F. S., Ladd, J. A. & Bower, W. W. Experimental and Computational Investigation of Supersonic Impinging Jets. *AIAA Journal* **40,** 599–609 (2002).
19. Kim, B. G., Yu, M. S., Cho, Y. I. & Cho, H. H. Distributions of Recovery Temperature on Flat Plate by Underexpanded Supersonic Impinging Jet. *Journal of Thermophysics and Heat Transfer* **16,** 425–431 (2002).
20. Kim, B., Cho, H. H. & Yu, M. Recovery Temperature Measurement of Underexpanded Sonic Jets Impinging on a Flat Plate. *Journal of Thermophysics and Heat Transfer - J THERMOPHYS HEAT TRANSFER* **17,** 313–319 (July 2003).
21. Yu, M. S., Kim, B. G. & Cho, H. H. Heat Transfer on Flat Surface Impinged by an Underexpanded Sonic Jet. *Journal of Thermophysics and Heat Transfer* **19,** 448–454 (2005).
22. Tian, Y., Li, W., Xue, P. & Gao, Z. Numerical Studies on Heat Transfer of Supersonic Combustion-Gas Jet Impingement on Perpendicular Flat Plate. *Heat Transfer Engineering* **43,** 864–878 (2022).
23. Schwamborn, D., Gerhold, T. & Heinrich, R. The DLR TAU-code: recent applications in research and industry (2006).
24. Wada, Y. & Liou, M.-S. *A flux splitting scheme with high-resolution and robustness for discontinuities* in *32nd Aerospace Sciences Meeting and Exhibit* (1994).
25. Thornber, B., Mosedale, A., Drikakis, D., Youngs, D. & Williams, R. An improved reconstruction method for compressible flows with low Mach number features. *Journal of Computational Physics* **227,** 4873–4894 (2008).
26. Wilcox, D. C. Reassessment of the scale-determining equation for advanced turbulence models. *AIAA Journal* **26,** 1299–1310 (1988).
27. Hannemann, V. *Numerical simulation of shock-shock-interactions considering chemical and thermal nonequilibrium* (DLR-Forschungsbericht 97-07, 1997).
28. Gerlinger, P., Moebius, H. & Brueggmann, D. An Implicit Multigrid Method for Turbulent Combustion. *Journal of Computational Physics* **167,** 247–276 (2001).
29. Hanemann, K., Schramm, J. M., Wagner, A., Karl, S. & Hanemann, V. *A Closely Coupled Experimental and Numerical Approach for Hypersonic and High Enthalpy Flow Investigations Utilising the HEG Shock Tunnel and the DLR TAU Code* tech. rep. (DLR, 2010).
30. Celik, I. B., Ghia, U., Roach, P. J., Freitas, C. J., Coleman, H. & Raad, P. E. Procedure for Estimation and Reporting of Uncertainty Due to Discretization in CDF Application. *Journal of Fluids Engineering - Transactions of the ASME* **130** (2008).
31. Zapryagaev, V., Kiselev, N. & Gubanov, D. Shock-Wave Structure of Supersonic Jet Flows. *Aerospace* **5,** 60 (June 2018).
32. McBride, B. J. & Gordon, S. *Computer Program for Calculation of Complex Chemical Equilibrium Compositions and Applications II. Users Manual and Program Description* tech. rep. (NASA Reference Publication (RP), 2013).
33. Perakis, N., Haidn, O. J. & Ihme, M. Heat transfer augmentation by recombination reactions in turbulent reacting boundary layers at elevated pressures. *International Journal of Heat and Mass Transfer* **178,** 121628 (2021).